ACS OMEGA

http://pubs.acs.org/journal/acsodf

Article

Computational Investigation of Near-Infrared-Absorbing Indeno[1,2-*b*]indole Analogues as Acceptors in Organic Photovoltaic Devices

Saleh S. Alarfaji,* Doua Fatima, Bakhat Ali, Abdul Sattar, Riaz Hussain,* Riaz Hussain, and Khurshid Ayub

Cite This: *ACS Omega* 2023, 8, 1430−1442

Read Online

ACCESS | Metrics & More | Article Recommendations

ABSTRACT: Organic solar cells (OSCs) with fullerene-free acceptors have recently been in high demand in the solar cell market because OSCs are less expensive, more flexible, long-lasting, eco-friendly, and, most importantly, have better photovoltaic performance with a higher PCE. We used INTIC as our reference R molecule and designed five new molecules DF1−DF5 from this R molecule. We attempted to test the power conversion efficiencies of five designed novel molecules, DF1−DF5. Therefore, we compared the PCE values of DF1−DF5 with that of R. We used a variety of computational techniques on these molecules to achieve this goal. Among the designed molecules, DF5 proved to be the best due to its lowest H−L bandgap energy E_g (1.82 eV), the highest value of λ_{max} (844.58 nm) within dichloromethane, the lowest excitation energy (1.47 eV), and the lowest oscillator strength value. The newly designed molecule DF2 exhibited the highest dipole moment (21.98 D), while DF3 displayed the minimum binding energy (0.34 eV) and the highest V_{oc} value (1.37 V) with $HOMO_{donor}$−$LUMO_{acceptor}$. According to the partial density of states (PDOS) and transition density matrix (TDM) analysis, DF2 and DF5 exhibited the best results. Charge-transfer (CT) analysis of the blend DF5 and PTB7-Th confirmed the accepting nature of the DF5 molecule. These findings show that by modifying the end-capped units, we can create customized molecules with improved photovoltaic properties. These findings also show that when compared with R, all of the designed molecules DF1−DF5 have improved optoelectronic properties. As a result, it is strongly advised to employ these conceptualized molecules in the practical synthesis of organic solar cells (OSCs).

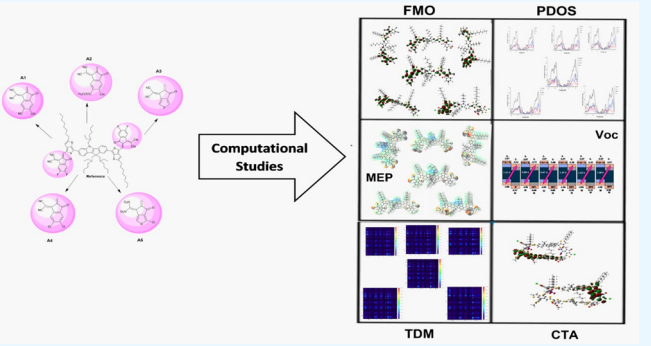

1. INTRODUCTION

For the past few decades, fossil fuels have remained the main source of energy, but the burning of fossil fuel causes many environmental problems. As a result, scientists have been working hard to reduce the rate of fuel consumption by replacing it with alternative energy sources. Solar cells (SCs) can be used as an alternative energy source. They can generate energy at a low cost and with fewer negative environmental consequences. It is primarily a renewable energy source. These SCs capture the sunlight energy and, in turn, produce electricity through the photovoltaic effect.[1−3] The first ever SC was made by Chapin et al. in Bell laboratories, and this SC had only a 6% power conversion efficacy. In the beginning, inorganic SCs were used for the purpose of generating electricity but they have some drawbacks. Therefore, researchers began to design and synthesize their counterparts, organic SCs, which are inexpensive, less toxic, lightweight, and solution processable.[4−6] The two main types of organic solar cells (OSCs) are fullerene-based OSCs and nonfullerene or fullerene-free OSCs. Fullerene-based OSCs were considered to be very efficient and have remained in the market for more than 20 years.[7] Later on, some limitations were found in the fullerene-based OSCs, such as high price, lower energy tunability, low flexibility, poor chemical modifications, and decreased photostability.[8] On the other hand, OSCs with fullerene-free acceptors have gained much attention of the world because they are highly compatible with polymer donor materials, energy tunable, less costly, transparent, and flexible in nature.[9−13]

Received: October 25, 2022
Accepted: December 16, 2022
Published: December 28, 2022

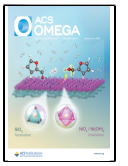

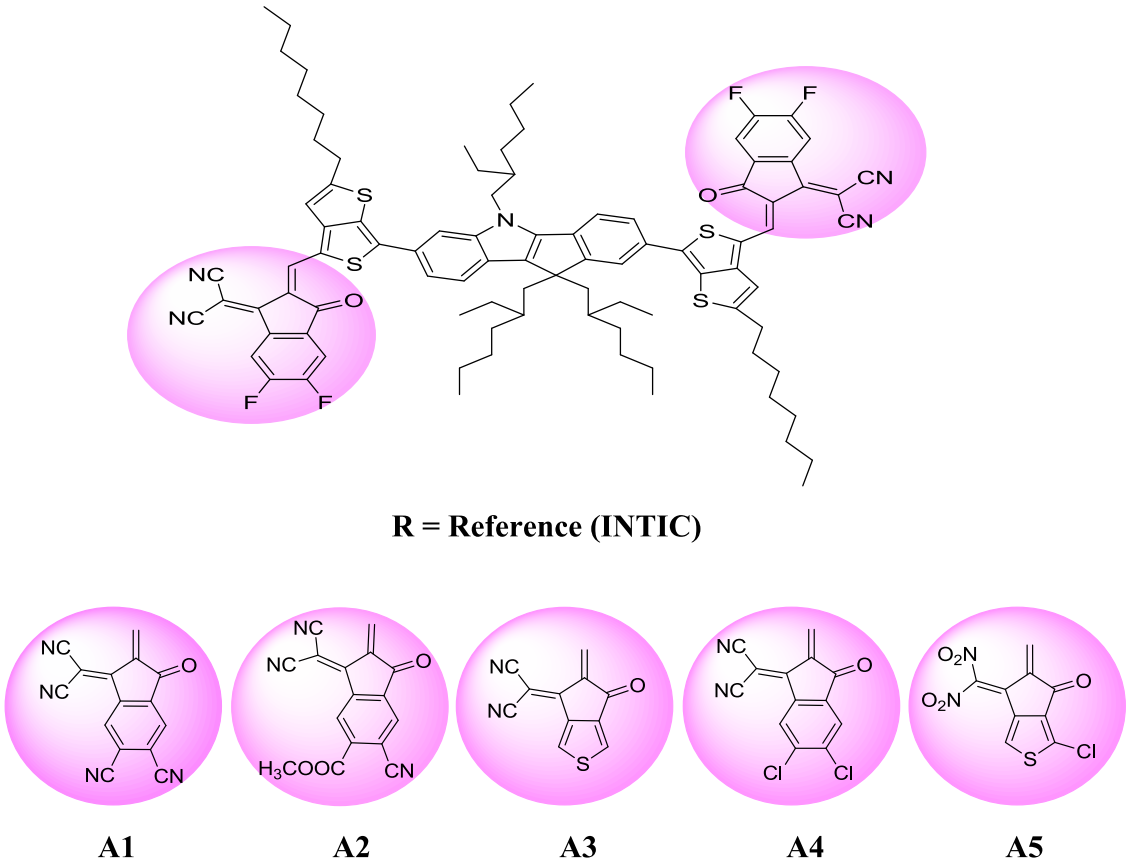

Figure 1. Chemical structures of R and the end-capped units A1−A5.

On the basis of symmetry, OSCs are divided into two main types, including symmetric and asymmetric NFA-based organic solar cells. Symmetric OSCs possess a C_2-type symmetry. They are considered less significant than asymmetric OSCs. Asymmetric OSCs possess many significant properties, such as strong optical absorption, a deeper lowest unoccupied MO, more molecular stacking, and, in turn, a higher PCE value. The asymmetric characteristic of the molecule increases with the unidirectional replacement technique, as a result of which the dipole moment of the molecule increases. Therefore, we chose a reference molecule with the asymmetry property. Hence, INTIC is our reference molecule R, which is asymmetric in nature. It contained indeno[1,2-*b*]indole (IN) as an electron-rich central core around which two pi-linkers and two acceptor units are present. Various strategies are available to improve the V_{oc}, J_{sc}, FF, and PCE values of OSCs, such as modifying the donor or acceptor region or preparing a fine blend of donor and acceptor materials. Here, the presence of pi-linkers and the introduction of more electron-withdrawing end-capped units enhance the π-stacking, which in turn increases the power conversion efficiency of OSCs. We designed five new molecules from the reference molecule R by introducing various EW end-capped units on its acceptor moieties. The newly designed end-capped units are named A1−A5. The newly designed project molecules are termed DF1−DF5. Our newly designed molecules showed greater bathochromic shifts and lower bandgap energies than the reference molecule R.

2. COMPUTATIONAL PROCEDURE

In the whole research procedure, all of the calculations were performed using Gaussian 09 program,[14] while all of the outcomes were imaged using Gauss View 5.0 program. We also used the latter-mentioned program to prepare input files for our research work. First of all, we optimized R by density functional theory (DFT) calculations at basis set 6−31G(d,p) and functional levels B3LYP, ωB97XD, CAM-B3LYP, and MPW1PW91. From the initially optimized.log file, we prepared an ultraviolet (UV) file of the R molecule. The solvent used for this purpose was dichloromethane. In this way, we obtained theoretical λ_{max} values for our reference R at four different functional levels. We compared all of the computed λ_{max} values of R with the experimental λ_{max} values.[15−22] Thus, we obtained the most appropriate functional level B3LYP/6−31G(d,p), which yielded very close results to the experimental λ_{max} values. Therefore, we used B3LYP as the functional level and 6−31G(d,p) basis set for more calculations of tailored molecules. Initially, the tailored molecules were optimized at B3LYP/6−31G(d,p), and then, we used these initially optimized files for further calculations. UV calculations for all of the designed molecules were carried out in the presence of dichloromethane as a solvent.[23] We used the same level of theory for molecules (R and DF1-DF5) to carry out further calculations such as the frontier molecular orbital (FMO), charge transfer (CT), partial density of states (PDOS), transition density matrix (TDM), and molecular electrostatic potential (MEP) analyses. Two programs PyMOlyze and Multiwfn were used to derive the results of PDOS and TDM, respectively. We also computed the energy of reorganization for the molecules (R and DF1−DF5). It has two main parts, including the external energy of reorganization (λ_{ext}) and the internal energy of reorganization (λ_{int}). λ_{ext} describes the external environmental relaxation and polarization effects.

https://doi.org/10.1021/acsomega.2c06878
ACS Omega 2023, 8, 1430−1442

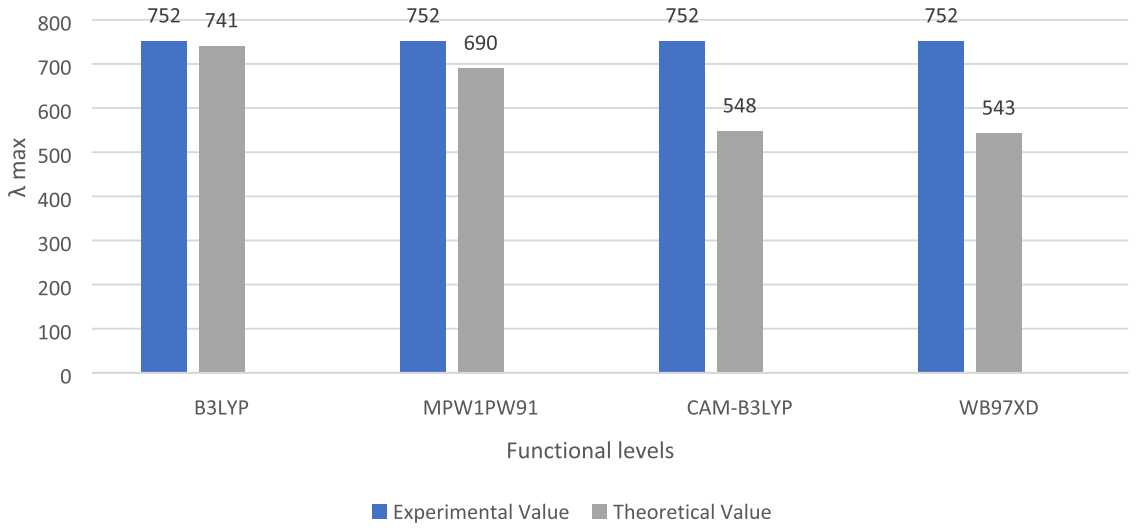

Figure 2. Comparison between experimental and theoretical λ_{max} values of R at four functional levels.

Similarly, λ_{int} describes the sudden variations that occur in the internal structure. Here, we ignore the effects of λ_{ext} and consider only the effects of λ_{int}. The energy of the reorganization for holes (λ_h) and electrons (λ_e) can be calculated by eqs i and ii

$$\lambda_h = [E_0^+ - E_+] + [E^0{}_+ - E_0] \quad \text{(i)}$$

$$\lambda_e = [E_0^- - E_-] + [E^0{}_- - E_0] \quad \text{(ii)}$$

In the above equations, the single point energies of the anion and cation can be measured using E_0^- and E_0^+, respectively. Energies of the optimized structures of the anion and cation can be measured by E^- and E^+, respectively. E_0 indicates the single point energy in the unexcited state. Anionic and cationic states energy of the neutral molecules are represented as E_-^0 and E_+^0, respectively.[24]

3. RESULTS AND DISCUSSION

In this study, INTIC is used as the reference R. INTIC contains an electron-rich aromatic core IN in it. By replacing the terminal units of the molecule R with five different acceptor moieties (A1−A5), we derived five new molecules that were named DF1−DF5 (Figure 1).

We tried to determine the optoelectronic properties of our project molecules (DF1−DF5) using various computational techniques.[25] We compared the results of DF1−DF5 with that R to identify the molecule that exhibited the best properties among all of these molecules. Initially, we calculated the theoretical absorption maxima (λ_{max}) of R in the dichloromethane solvent at four different functional levels (B3LYP, MPW1PW91, WB97XD, and CAM-B3LYP) and basis set 6−31G(d,p), which is given in Figure 2.

This experimental λ_{max} value for R is 752 nm in the chloroform solvent. We compared both the experimental and theoretical λ_{max} values of R. Hence, we found that B3LYP with the basis set 6−31G(d,p) remained the most appropriate. For further calculations, we selected the above-discussed level of DFT at 6−31G(d,p).

3.1. Frontier Molecular Orbital Analysis. The optimized diagrams of R and DF1−DF5 showed that all of the molecules are planar in structure. A planar structure is an important property for better charge mobility. The distribution pattern of electrons in the molecules (R and DF1−DF5) is represented by FMO. Figure 3 shows the structures for the highest occupied MOs and the lowest unoccupied MOs of R and DF1−DF5.

In the HOMO of R, the electron density is largely located on the D region. The LUMO of R indicates that some of the electron density is present on π-spacers but largely situated in the A region. Other molecules, such as DF1, DF2, and DF4, also exhibit the same effect on the HOMO and LUMO. In the HOMO of these molecules, the electron density is mainly concentrated on the D region and a very small electron density is found on the A region. On the other hand, in the LUMO of these molecules, the electron density is mostly concentrated on the benzene ring and the end-capped units. The molecules DF3 and DF5 exhibited somewhat different electron density distribution patterns on the HOMO and LUMO regions. In the HOMOs of these molecules (DF3 and DF5), the electron density is mostly distributed on the D region and significantly present on the pi-linkers and A regions. In the LUMOs of these molecules (DF3 and DF5), a very small electron density is present on the pi-linkers, but most of the electron density is present on the whole acceptor regions. Both of these molecules contain a thiophene ring as their acceptor moiety. The existence of a thiophene ring and the highly electron-withdrawing end-capped units increases the electron density of the molecules DF3 and DF5 on the acceptor region of their LUMOs (Figure 4).

We generalized that in the HOMOs of R and DF1−DF5, the electron density is largely distributed on the D regions. In the LUMOs of R and DF1−DF5, some of the electron density is present on the pi-linkers, but it is mostly located on the A regions. This indicates the transportation of electrons from the HOMO of the D region to the LUMO of the A region in all of the molecules (R and DF1A's DF5), especially in the tailored molecules DF1−DF5. This phenomenon illustrates the electron-withdrawing nature of the acceptor moieties. Hence, a highly EW nature of the end-capped units of the acceptor moieties is very efficient for the proper flow of electron density from the D to the A region of the molecules. The computed HOMO, LUMO, and E_g energy for R and DF1−DF5 are presented in Table 1.

https://doi.org/10.1021/acsomega.2c06878
ACS Omega 2023, 8, 1430−1442

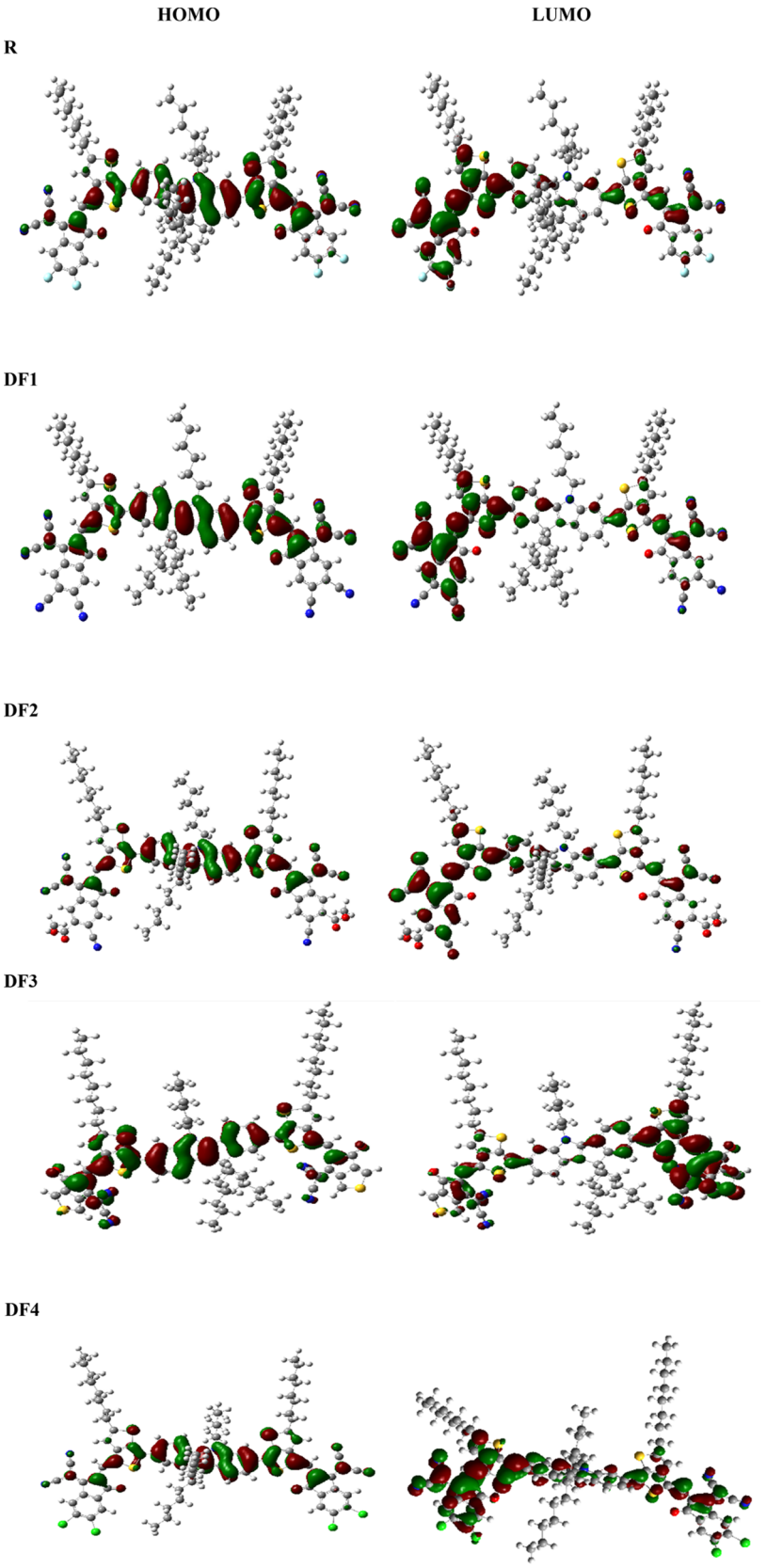

Figure 3. continued

https://doi.org/10.1021/acsomega.2c06878
ACS Omega 2023, 8, 1430−1442

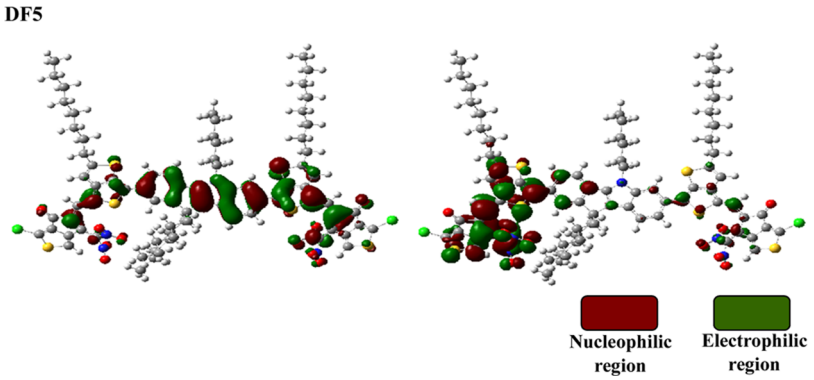

Figure 3. FMO structures for all of the molecules, including R and DF1−DF5.

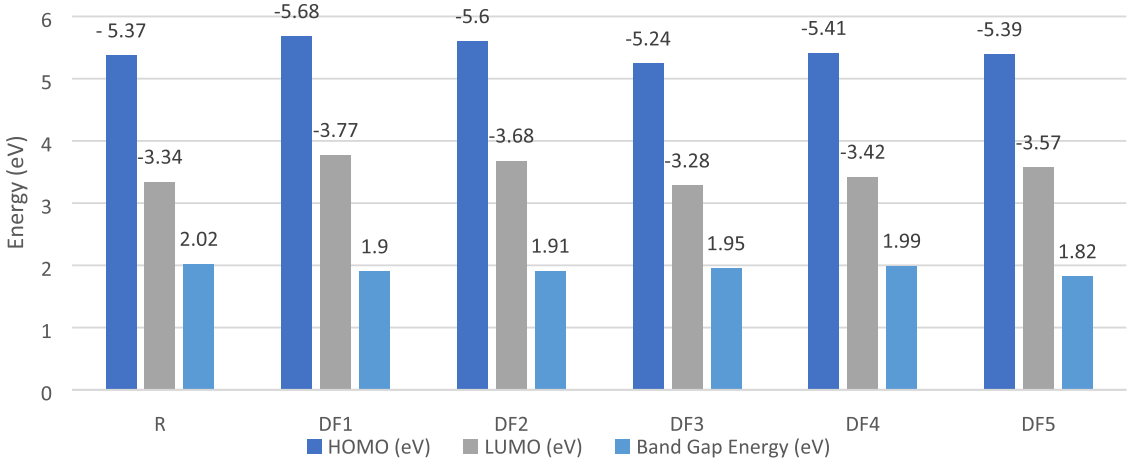

Figure 4. Graph for the HOMO, LUMO, and E_g values.

Table 1. HOMO, LUMO, and Bandgap Energies for All of the Molecules R and DF1−DF5

molecules	E_{HOMO} (eV)	E_{LUMO} (eV)	E_g (eV)
R	−5.37	−3.34	2.02
DF1	−5.68	−3.77	1.90
DF2	−5.60	−3.68	1.91
DF3	−5.24	−3.28	1.95
DF4	−5.41	−3.42	1.99
DF5	−5.39	−3.57	1.82

The computed HOMO values for the molecules (R and DF1−DF5) are −5.37 (R), −5.68 (DF1), −5.60 (DF2), −5.24 (DF3), −5.41 (DF4), and −5.39 eV (DF5), respectively. The computed LUMO values for the molecules (R and DF1−DF5) are −3.34 (R), −3.77 (DF1), −3.68 (DF2), −3.28 (DF3), −3.42 (DF4), and −3.57 eV (DF5), respectively. The estimated E_g energies of H−L for the molecules (R and DF1−DF5) are 2.02 (R), 1.90 (DF1), 1.91 (DF2), 1.95 (DF3), 1.99 (DF4), and 1.82 eV (DF5), respectively. The reference molecule R possesses two fluorine atoms, an oxygen atom, and cyano groups as end-capped units. DF1 contains cyano groups and an oxygen atom, while DF2 contains an oxygen atom, a cyano group, and an acetate group as end-capped units. A thiophene ring, oxygen atom, and cyano groups are present in the DF3 molecule. The molecule DF4 possesses cyano groups, an oxygen atom, and chlorine atoms in it. The end-capped units present on the DF5 molecule include an oxygen atom, a chlorine atom, nitro groups, and a thiophene ring. Among all of these molecules, DF3 showed the lowest value for the HOMO and the LUMO due to the existence of the thiophene ring as an end-capped unit in it. This thiophene ring stabilizes its structure.

By analyzing the bandgap energy, we found an increasing order of the bandgap energy as follows: R > DF4 > DF3 > DF2 > DF1 > DF5. Here, we realized that all of the engineered molecules DF1−DF5 have smaller E_g values than R. However, the engineered molecule DF5 exhibited the lowest value of E_g among all of the molecules due to the presence of the highly electron-withdrawing oxygen atom, chlorine atom, thiophene ring, and nitro groups as end-capped units on its acceptor regions. It is beneficial to have a low E_g value of a molecule. This is only because the molecule that possesses a low E_g value utilizes some of its absorbed energy to become excited and most of its energy to produce electricity. Therefore, we can conclude that DF5 is the best tailored molecule to enhance the efficiency of an OSC.

3.2. Partial Density of States. PDOS is another important analysis executed on DF1−DF5 and R at B3LYP/6−31G(d,p). It is a factual demonstration of FMO. It is clear from the figures of HOMO, LUMO, and PDOS that the electron density has been shifted from the donor to the acceptor regions in all of the molecules (R and DF1−DF5) due to the strongly EW nature of the end-capped units.

Figure 5 shows that two crests are present along the two sides of the graphs, and a trough is present between the two crests in each graph. The peak along the left side of the graph represents the HOMO region of the donor, and the peak on

https://doi.org/10.1021/acsomega.2c06878
ACS Omega 2023, 8, 1430−1442

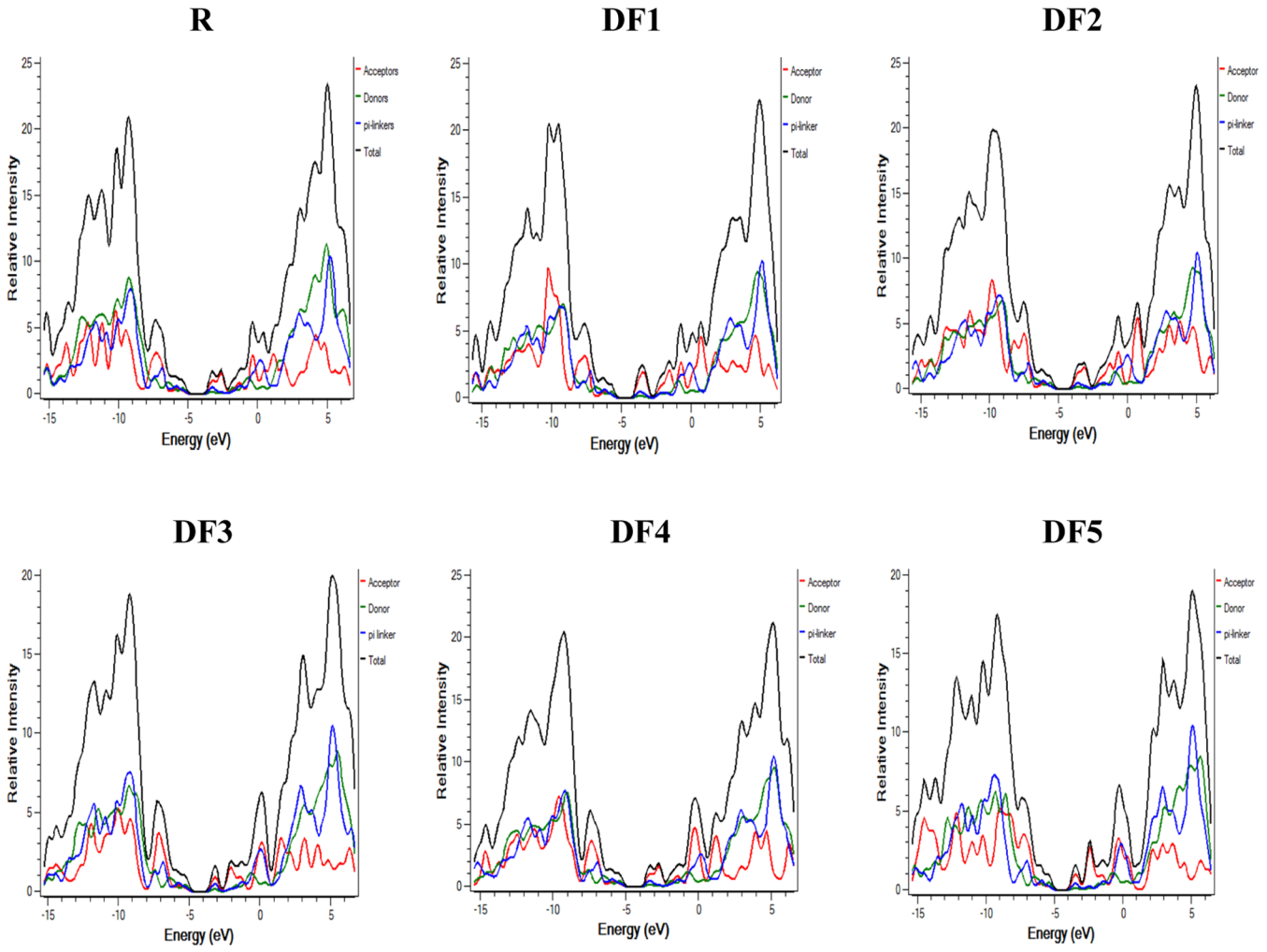

Figure 5. Graphs of PDOS for R and DF1−DF5 molecules at DFT.

the other side represents the LUMO of the acceptor. In each graph, red, green, and blue lines are present, which symbolize the acceptor, donor, and pi-linkers, respectively. As in photovoltaic materials, the HOMO behaves as a valence band, and the LUMO behaves as a conduction band. Therefore, our major concern is regarding the conduction of charge, i.e., electrons. Hence, enhancement in photovoltaic properties can be described on the basis of the electron density in the acceptor in the LUMO region.

Hence, we can conclude that in all of the architectured molecules (DF1−DF5), electrons display a delocalization pattern. As a result, a large amount of electron density has been transmitted from the HOMO of the D region to the LUMO of the A region in all of the molecules, especially in the DF1−DF5 molecules. According to PDOS, the increasing order of maximum charge density transportation from the HOMO of the D region to the LUMO of the A region is as follows: R < DF3 < DF5 < DF1 < DF4 < DF2. This order indicates that all of the architectured molecules DF1−DF5 displayed better charge transfer from D to A as compared with R. Thus, we can conclude that all of the studied molecules DF1−DF5 strongly contain EW end-capped units, which can prove beneficial for the efficient designing and working of an OSC.

3.3. Molecular Electrostatic Potential. MEP diagrams demonstrate the dispersion of charges in the molecules (R and DF1−DF5) three-dimensionally. MEP surfaces also categorize the electron-rich and electron-deficient parts of these molecules.[26] MEP structures for R and DF1−DF5 are shown in Figure 6. All of the MEP surfaces exhibit the same color scheme. Each MEP diagram consists of three colors, red, blue, and green, which represent the highly electron-deficient, electron-rich, and neutral parts of the molecules (R and DF1−DF5), respectively.

The red color with the negative extreme (lowest) electrostatic potential demonstrates the electrophilic nature of the end-capped units. Therefore, these end-capped units act as good acceptors due to their electron-withdrawing nature. On the other hand, the blue color with the positive extreme (highest) electrostatic potential shows the nucleophilic nature of the central donor part. The green part denotes the neutral position. It is clear from Figure 6 that all of the MEP diagrams of the molecules R and DF1−DF5 exhibit almost similar electrostatic potential distribution patterns. This shows that all of the project molecules are very efficient for the better functioning of OS cells.

3.4. Optical Properties. UV−visible (UV−vis) analysis is used to determine the photophysical and optoelectronic characteristics of R and DF1−DF5. Here, we used the CPCM model in which dichloromethane is used as a solvent at TD-SCF along with B3LYP/6−31G(d,p) for R and DF1−DF5 molecules. In this way, we determined the theoretical λ_{max}

https://doi.org/10.1021/acsomega.2c06878
ACS Omega 2023, 8, 1430−1442

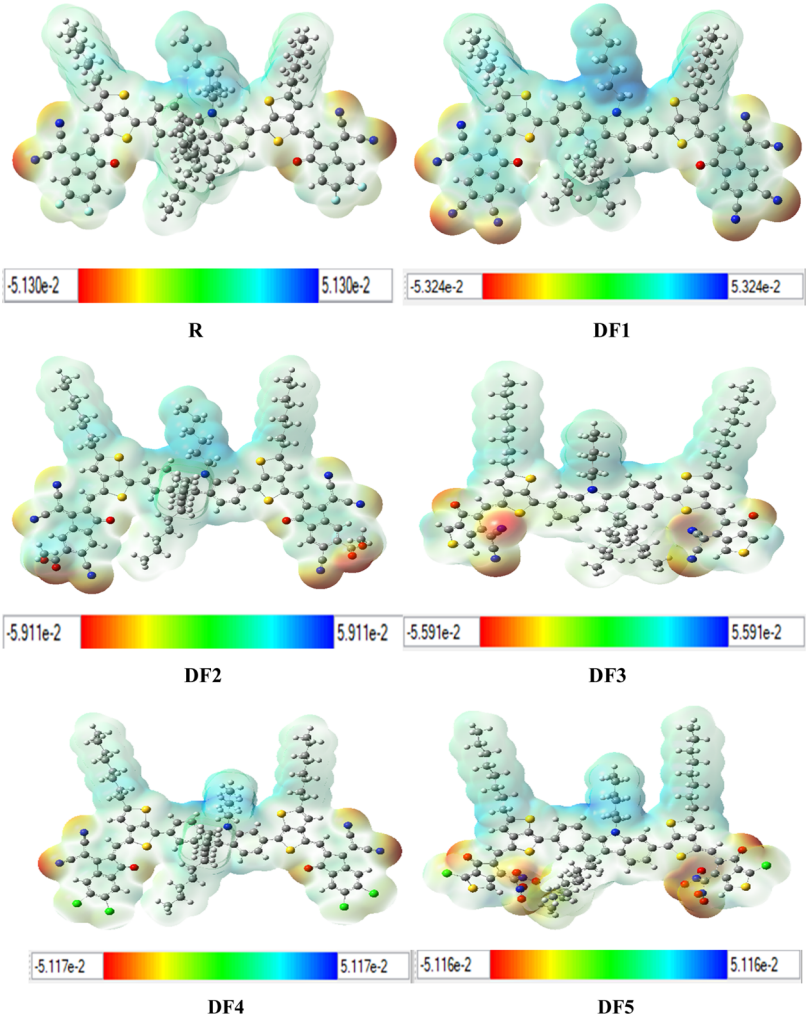

Figure 6. Molecular electrostatic potential (MEP) analysis of R and DF1−DF5.

Table 2. Experimentally Recorded and DFT-Based λ_{max}, Excitation Energy, Oscillator Strength, MO Assignments, and Dipole Moment

molecule S	calculated λ_{max} (nm)	experimental λ_{max}	exc. (eV)	osc. strength (f)	assignment	dipole moment
R	741.3105711	752 (chloroform)	1.67	2.1191	HOMO->LUMO (97%)	7.6432
DF1	805.6676393		1.53	1.756	HOMO->LUMO (97%)	20.3421
DF2	799.2276994		1.55	1.8628	HOMO->LUMO (97%)	21.9796
DF3	767.3713747		1.61	1.4694	HOMO->LUMO (97%)	14.5423
DF4	759.195352472		1.63	2.1149	HOMO->LUMO (97%)	9.4804
DF5	844.578971473		1.47	1.1652	HOMO->LUMO (98%)	16.3281

value for R and DF1−DF5, whereas the experimental λ_{max} value of the reference R was calculated in the solvent chloroform. Therefore, we compared the experimental and theoretical λ_{max} values of R, as shown in Table 2.

In the gaseous phase calculation, no gaseous solvent is used, and the gaseous phase calculation is performed in a vacuum environment.

From the above table, we found 741.31 nm as the λ_{max} value of R. The λ_{max} values for DF1−DF5 are found to be 805.66, 799.22, 767.37, 759.19, and 844.58 nm, respectively. The ascending order of λ_{max} values is as follows: DF5 > DF1 > DF2 > DF3 > DF4 > R. Among all of these molecules (R and DF1−DF5), R displayed the lowest λ_{max} value and it contained two fluorine atoms as end-capped units, whereas the molecule DF5 exhibited the highest λ_{max} value with a large bathochromic shift. The molecule DF5 might display this large bathochromic shift due to the existence of the highly EW chlorine atom, nitro groups, and thiophene ring as its end-capped units. The extended π-conjugation of the thiophene ring can be a reason for this large λ_{max} value. DF1 showed a greater λ_{max} value than DF2 due to the presence of a different end-capped unit in only one position. DF1 contains four cyano groups as end-capped units, whereas DF2 contains only three cyano groups and one acetate group instead of a fourth cyano group. DF3 exhibited a greater λ_{max} value than DF4 because DF3 contains a thiophene ring with extended π-conjugation and a greater EW effect, whereas DF4 contains a benzene ring with two chlorine atoms on it as end-capped units. As all of the studied molecules DF1−DF5 revealed greater λ_{max} values than R, we can conclude that all of the studied molecules are very efficient

https://doi.org/10.1021/acsomega.2c06878
ACS Omega 2023, 8, 1430−1442

for the better functioning of OSCs. Its computer-generated spectral representation is given in Figure 7. This also indicates

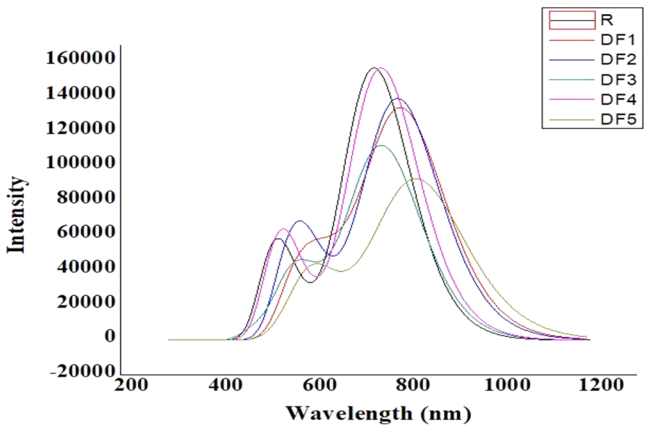

Figure 7. Computer-generated absorption spectra of all of the studied molecules R and DF1−DF5 in the dichloromethane solvent.

that DF5 is the best tailored molecule. The previous literature on SCs demonstrates that if the molecules have higher absorption maxima in the bathochromic region, then they conduct current efficiently, enhance the J_{sc} value, and improve the photoconduction ability. Moreover, if the bandgap energy is decreased, then more electrons are produced in the visible area, which in turn transfer the λ_{max} value toward higher wavelengths. This can then increase the V_{oc} value, which as a result enhances the PCE value of OSCs.[27−29]

Excitation energy is also called transition energy. The ascending order of excitation energy for the molecules (R and DF1−DF5) is DF5 < DF1 < DF2 < DF3 < DF4 < R. This order is quite similar to that of the H−L bandgap energy. Electronic transitions become efficient from the HOMO of the D region to the LUMO of the A region if the energy of excitation is low. Again, according to the excitation energy results, the project molecule DF5 remained the best molecule as it displayed the lowest excitation energy (1.47 eV) among all of the molecules (R and DF1−DF4).

Oscillator strength is the phenomenon of a molecule absorbing or emitting electromagnetic radiation during transitions in different energy levels. It is denoted by the symbol f. Molecule R exhibited the maximum oscillator strength as compared with all of the tailored molecules (DF1−DF5). DF5 displayed the lowest value of f. Thus, we can conclude that all of the tailored molecules showed very good oscillator strength properties, but the molecule DF5 displayed the best properties among all others.

3.5. Dipole Moment. The dipole moment is a significant parameter to determine the efficiency of OSCs. In our research, we computed the dipole moment of R and DF1−DF5 at the same functional level of DFT in a solvent (dichloromethane). On increasing the dipole moment value of a molecule, its solubility in an organic solvent increases. We used dichloromethane as the organic solvent. The dipole moment values for R, DF1, DF2, DF3, DF4, and DF5 are 7.64, 20.34, 21.98, 14.54, 9.48, and 16.32 D, respectively. Table 2 shows that the dipole moment value increases in the order R < DF4 < DF3 < DF5 < DF1 < DF2. This order indicates that all of the engineered molecules (DF1−DF5) have higher dipole moment values relative to R. This means that all of the engineered molecules (DF1−DF5) have higher solubility in organic solvents such as dichloromethane. However, the molecule DF2 exhibits the highest dipole moment, which indicates its extraordinary property of film morphology. The dipole moment of DF2 is maximum because of the existence of cyano groups as well as acetate groups. Also, the other designed molecules exhibit a higher dipole moment as compared with the reference, but they show different behaviors due to their different acceptor groups, as shown in Figure 8, which displays a schematic sketch of the whole designed project. The greater the dipole moment, the greater will be the polarity, and the greater will be the chances for the flow of charges. The faster the charges flow, the higher will be the PCE of the solar cell. Molecules of BHJ OSCs mostly exhibit higher dipole moment values. In such molecules, two dipoles are present in an anti-parallel fashion, which directly enhances their crystallinity. Moreover, a higher dipole moment value decreases the disorder between D and A, which in turn improves the charge mobility between D and A.

3.6. Reorganization Energy. The reorganization energy is another significant tool to understand the efficacy of OSCs. It is associated with charge mobilities such as electrons and holes. The energy of reorganization and charge mobilities are inversely proportional to each other.[30] If the energy of reorganization of the D molecule decreases, then the rate of charge transfer becomes higher.[31] The energy of reorganization is greatly affected by the cationic and anionic geometry. The geometry of anions indicates the transfer of electrons from the D material, while, on the other hand, the geometry of cations represents holes. Two forms of reorganization energies exist,

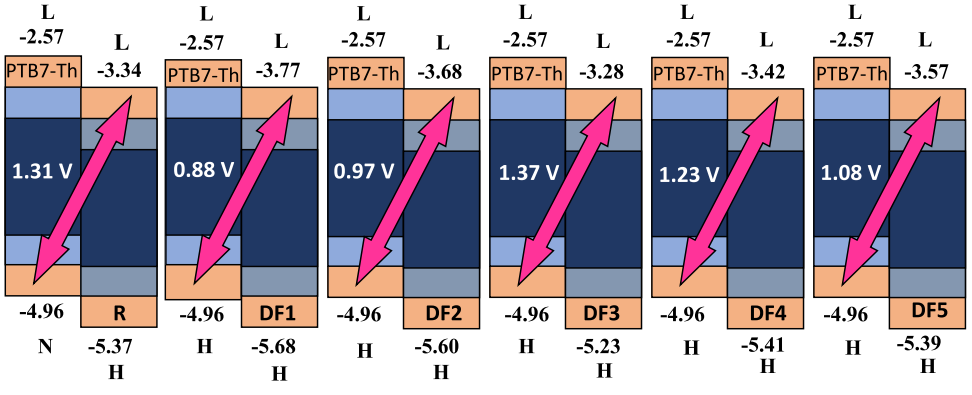

Figure 8. Voc diagram of R and DF1−DF5 acceptors with the PTB7-Th donor.

https://doi.org/10.1021/acsomega.2c06878
ACS Omega 2023, 8, 1430−1442

i.e., internal and external reorganizational energies. Here, we ignore the external reorganization energy due to the influence of the external environment and consider only the internal reorganization energy. The computed reorganizational energy for DF1−DF5 and R by DFT is presented in Table 3.

Table 3. Reorganizational Energy of R and Architectured Molecules (DF1−DF5) Computed at B3LYP, 6−31G(d,p)

molecules	λ_e (eV)[a]	λ_h (eV)[b]
R	0.0054	0.0062
DF1	0.0035	0.0061
DF2	0.0043	0.0064
DF3	0.0075	0.0062
DF4	0.0046	0.0058
DF5	0.0094	0.0072

[a]Reorganizational energy of electrons. [b]Reorganizational energy of holes.

Among these molecules, DF1 displayed the lowest λ_e value, which indicates its highest charge mobility rate.

3.7. Open-Circuit Voltage. Another promising tool used to describe the efficacy of OSCs is V_{oc}.[32] It provides information about the current that can be produced by an optical instrument.[24] The highest amount of voltage of any device at its null current is called V_{oc}. It is related to two types of currents, i.e., photogenerated current and saturation voltage. To achieve better efficiency of OSCs, we should have greater value of V_{oc} with a decreased value of the HOMO level of the D molecule and an increased value of the LUMO level of the A moiety.[33] Figure 9 demonstrates the open-circuit voltage values of R and all newly designed molecules.

We used PTB7-Th as the donor material for our research. Therefore, we prepared a blend of R and DF1−DF5 with PTB7-Th. The V_{oc} values for the molecules (R and DF1−DF5) can be calculated using the Scharber and colleagues' equation[34] given below

$$V_{OC} = (E^{D}_{HOMO} - E^{A}_{LUMO}) - 0.3 \quad \text{(iii)}$$

The difference in V_{oc} results of molecules (R and DF1−DF5 with PTB7-Th donor) is given in the Figure 8. The increasing order of V_{oc} values is as follows: DF3 > R > DF4 > DF5 > DF2 > DF1. A greater value of V_{oc} facilitates greater charge transportation. Thus, greater will be the PCE of the photovoltaic material. Thus, the molecule DF3 with a V_{oc} value of 1.37 V showed the best results.

3.8. Transition Density Matrix and Binding Energy. TDM helps investigate the type of transition from S_0 to S_1 of the molecules R and DF1−DF5 at the above-mentioned functional level and basis set.[20,35−38] There is very little contribution of hydrogen atoms in such transitions. Therefore, we ignore the impact of hydrogen atoms in this study. TDM is employed to determine the localization of electrons and holes in the excited states and to understand the behavior of A and D in such states. To assess the TDM graphs, we divide R and the engineered molecules DF1−DF5 into three parts, including donor, pi-linker, and acceptor (D, P, and A, respectively). TDM graphs are given in Figure 10.

We used the diagonal method to study these graphs. It is confirmed from TDM graphs that the flow of electrons occurred toward A from the D region. The increasing order of electronic distribution from the D to A region is as follows: R < DF1 < DF2 < DF4 < DF3 < DF5. Thus, all of the designed molecules DF1−DF5 exhibited better charge transfer from the D to the A region compared with the reference molecule R. However, the tailored molecule DF5 exhibited the greatest orientation of electrons toward A from the D region, which is our main focus. Here, it is important to note that the charge separation ability of all of the investigated molecules DF1−DF5 is greater than that of R, which indicates the better current charge density J_{sc} of these planned molecules (DF1−DF5).

The binding energy E_b provides significant information to improve the efficiency of OSCs. E_b depends on the Coulombic interactions and exciton detachment. The greater the value of E_b, the greater will be the interaction among opposite charges, the lesser will be the charge separation, and vice versa. The E_b values of R and DF1−DF5 can be evaluated from eq iv.

$$E_b = E_{H-L} - E_{opt} \quad \text{(iv)}$$

In the above equation, E_b, E_{H-L}, and E_{opt} symbolize the binding energy, the bandgap energy, and the single point energy of the molecules, respectively. These energies are given in Table 4.

A higher E_b value means lower charge separation. It is clear from Table 4 that the molecule DF3 exhibited the lowest E_b

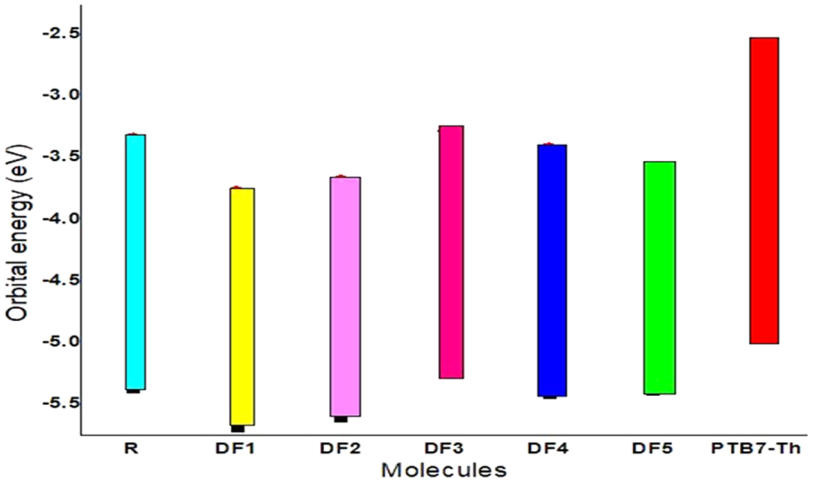

Figure 9. Molecular orbital diagram of R and engineered molecules DF1−DF5 with PTB7-Th.

https://doi.org/10.1021/acsomega.2c06878
ACS Omega 2023, 8, 1430−1442

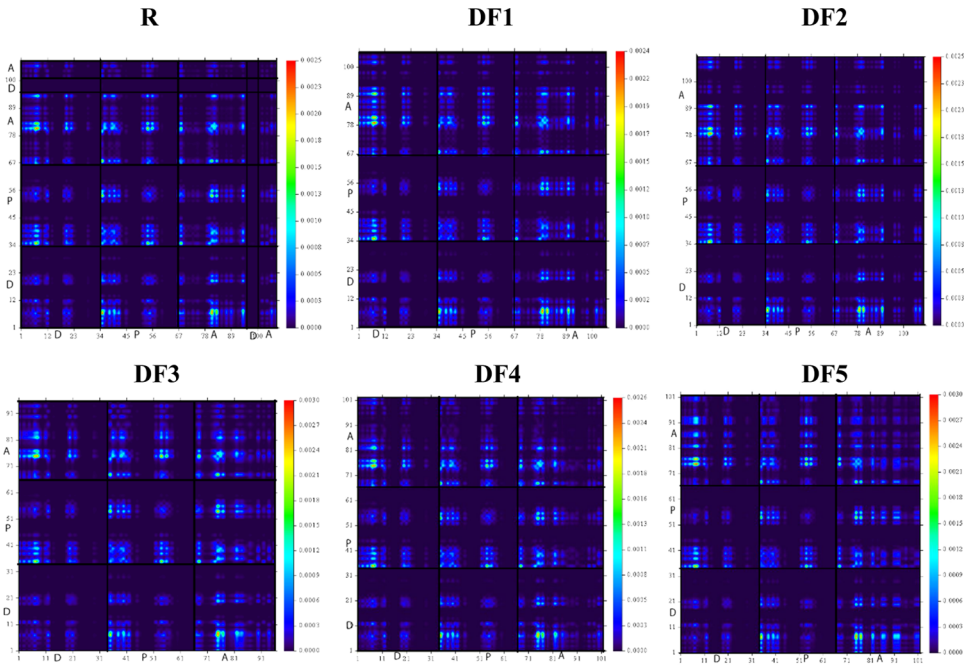

Figure 10. TDM diagrams for R and the architectured molecules DF1−DF5 in the S1 state.

Table 4. Computed Binding Energy Values of R and DF1−DF5 at B3LYP/6−31G(d,p)

molecules	E_{H-L}	E_{opt}	E_b
R	2.02	1.67	0.35
DF1	1.90	1.53	0.37
DF2	1.91	1.55	0.36
DF3	1.95	1.61	0.34
DF4	1.99	1.63	0.36
DF5	1.82	1.47	0.35

value, which indicates the greatest charge-transfer ability of the DF3 molecule.

3.9. Complex DF5 with PTB7-Th for Charge Transfer (CT) Analysis. A complex of DF5/PTB7-Th is examined to understand its change-transfer pattern. The reason for choosing PTB7-Th is that it is one of the best and most suitable donor molecules for confirming whether a molecule is an acceptor or not. Among all of the engineered molecules (DF1−DF5), we prepared a blend of acceptor DF5 with the donor polymer PTB7-Th due to the lowest E_g value, highest λ_{max} value, and other important features of DF5. The optimized geometry of DF5 and PTB7-Th is obtained through the same functional level of DFT-based calculations. This optimized structure of DF5 and PTB7-Th is given in Figure 11. To understand the flow of charge from the D to the A unit, we carried out the FMO analysis of DF5 and PTB7-Th at the same basis set of DFT. The HOMO and LUMO structures of the complex (DF5 and PTB7-Th) are given in Figure 12. It is clear from Figure 12 that the density of charges has shifted from the donor to the acceptor part. Thus, the acceptor-type nature of the molecule DF5 was confirmed.

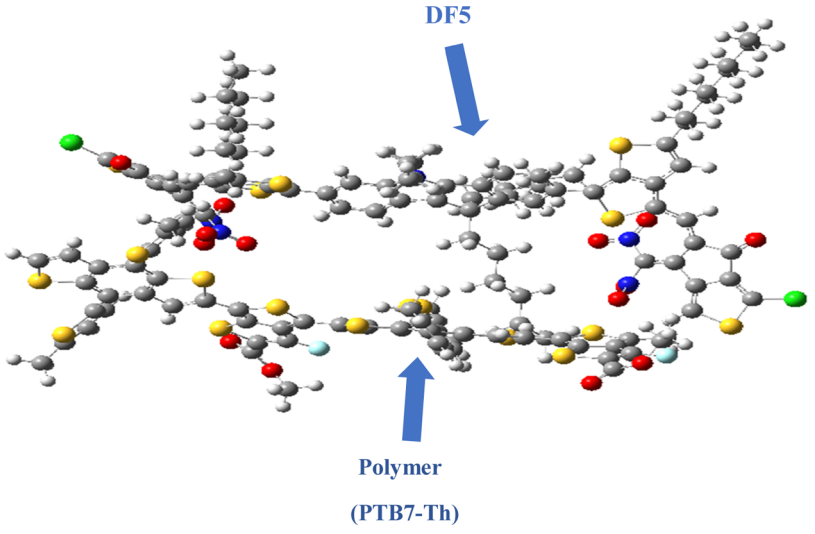

Figure 11. Geometry of the Complex PTB7-Th with DF5.

https://doi.org/10.1021/acsomega.2c06878
ACS Omega 2023, 8, 1430−1442

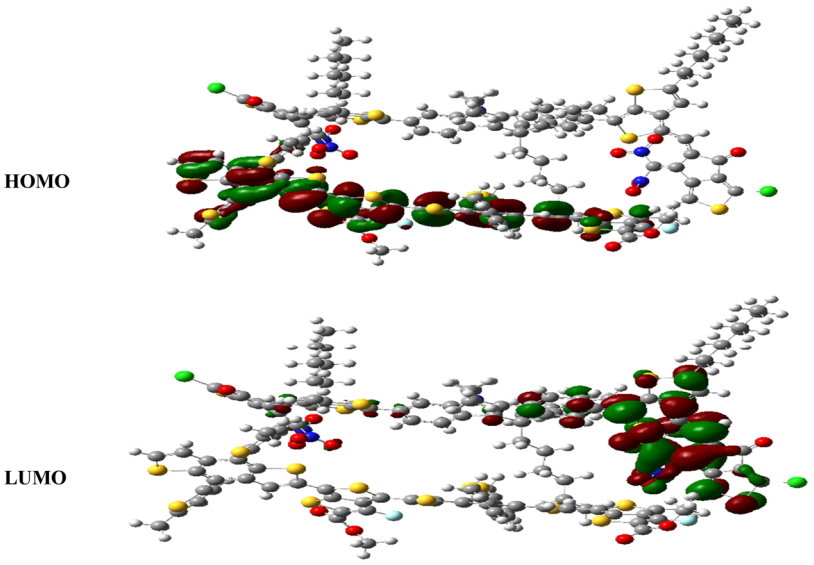

Figure 12. HOMO and LUMO of the complex PTB7-Th/DF5.

4. CONCLUSIONS

Five new NFAs DF1−DF5 are tailored from R (INTIC) by altering its end-capped units. The main purpose of planning and designing these molecules (DF1−DF5) is to obtain OSCs with improved optoelectronic and photovoltaic properties. Several computational techniques have been applied to understand the efficiency of the reference R vs the engineered molecules (DF1−DF5). It is clear that all of the engineered molecules DF1−DF5 have lower bandgap energies (1.82−1.99 eV) as compared with R (2.02 eV). The molecule DF5 exhibited excellent results with the lowest E_g value (1.82 eV). According to UV−vis calculations, DF1−DF5 (λ_{max} = 759.19−844.58 nm) displayed a red shift relative to R (λ_{max} = 741.31 nm) in dichloromethane solvent. The tailored molecule DF5 displayed significant results in terms of the absorption maxima, excitation energy, and oscillator strength due to its extended conjugation and strongly EW end-capped units. The reorganization energy indicates that the molecule DF1 exhibits the maximum charge mobility rate. In the V_{oc} diagram, all of the molecules (R and DF1−DF5) are blended with the polymer donor PTB7-Th to investigate the most efficient blend. The architectured molecules with reduced binding and reorganization energies revealed exceptional photovoltaic characteristics. To perfectly understand the transportation of charge, we inspected a complex of PTB7-Th with DF5. It is concluded that all of the tailored molecules (DF1−DF5) with modified end-capped units displayed enhanced optoelectronic characteristics compared with R. Hence, it is strongly suggested that the investigated molecules DF1−DF5 must be used in OSCs to boost the efficiency of such devices.

AUTHOR INFORMATION

Corresponding Authors

Saleh S. Alarfaji − *Department of Chemistry, Faculty of Science, King Khalid University, Abha 61413, Saudi Arabia; Research center for Advanced Materials Science (RCAMS), King Khalid University, Abha 61514, Saudi Arabia;* orcid.org/0000-0001-7297-7185; Email: ssalarvagi@kku.edu.sa

Riaz Hussain − *Department of Chemistry, Division of Science and Technology, University of Education, Lahore 32200, Pakistan;* orcid.org/0000-0002-6154-1244; Email: riaz.hussain@ue.edu.pkk

Authors

Doua Fatima − *Department of Chemistry, Division of Science and Technology, University of Education, Lahore 32200, Pakistan*

Bakhat Ali − *Institute of Chemistry, Khwaja Fareed University of Engineering & Information Technology, Rahim Yar Khan 64200, Pakistan*

Abdul Sattar − *Department of Chemistry, Division of Science and Technology, University of Education, Lahore 32200, Pakistan*

Riaz Hussain − *Department of Chemistry, University of Okara, Okara 56300, Pakistan;* orcid.org/0000-0003-4304-0451

Khurshid Ayub − *Department of Chemistry, COMSATS Institute of Information Technology, Abbottabad 22060, Pakistan;* orcid.org/0000-0003-0990-1860

Complete contact information is available at: https://pubs.acs.org/10.1021/acsomega.2c06878

Notes

The authors declare no competing financial interest.

ACKNOWLEDGMENTS

S.S.A. appreciates the Deanship of Scientific Research at King Khalid University for funding this work through the Large Group Research Project under grant number 34/43 and also acknowledges the Research Center for Advance Materials (RCAMS) at King Khalid University, Saudi Arabia for their valuable technical support

REFERENCES

(1) Kanwal, N.; Hussain, R.; Sattar, A.; Assiri, M. A.; Imran, M.; Hussain, A.; Yawer, M. A.; Hussain, R.; Mehboob, M. Y.; Khalid, M.; Ayub, K.; Hassan, T. DFT based modeling of asymmetric non-fullerene acceptors for high-performance organic solar cell. *Opt. Quantum Electron.* **2022**, *54*, No. 546.

(2) Khan, S.; Hussain, R.; Satar, A.; Assiri, M. A.; Imran, M.; Hussain, A.; Yawer, M. A.; Hussain, R.; Mehboob, M. Y.; Sumrra, S. H.; Khalid, M.; Ayub, K. Quantum chemical designing of novel

https://doi.org/10.1021/acsomega.2c06878
ACS Omega 2023, 8, 1430−1442

fullerene-free acceptor molecules for organic solar cell applications. *J. Mol. Model.* **2022**, *28*, No. 67.
(3) (a) Mehboob, M. Y.; Khan, M. U.; Hussain, R.; Ayub, K.; Sattar, A.; Ahmad, M. K.; Irshad, Z.; Saira; Adnan, M. Designing of benzodithiophene core-based small molecular acceptors for efficient non-fullerene organic solar cells. Spectrochim. *Spectrochim. Acta, Part A* **2021**, *244*, No. 118873. (b) Chapin, D. M.; Fuller, C. S.; Pearson, G. L. A New Silicon p-n Junction Photocell for Converting Solar Radiation into Electrical Power. *Journal of Applied Physics* **1954**, *25* (5), 676−677.
(4) Lu, L.; Zheng, T.; Wu, Q.; Schneider, A. M.; Zhao, D.; Yu, L. Recent advances in bulk heterojunction polymer solar cells. *Chem. Rev.* **2015**, *115*, 12666−12731.
(5) Li, G.; Zhu, R.; Yang, Y. Polymer solar cells. *Nat. Photonics* **2012**, *6*, 153−161.
(6) Lee, J.; Lee, S. M.; Chen, S.; Kumari, T.; Kang, S. H.; Cho, Y.; Yang, C. Organic photovoltaics with multiple donor−acceptor pairs. *Adv. Mater.* **2019**, *31*, No. 1804762.
(7) Liu, T.; Troisi, A. What makes fullerene acceptors special as electron acceptors in organic solar cells and how to replace them. *Adv. Mater.* **2013**, *25*, 1038−1041.
(8) Subramanyam, B. V. R. S.; Mahakul, P. C.; Sa, K.; Raiguru, J.; Mahanandia, P. Investigation of improvement in stability and power conversion efficiency of organic solar cells fabricated by incorporating carbon nanostructures in device architecture. *J. Phys.: Mater.* **2020**, *3*, No. 045004.
(9) He, Y.; Li, Y. Fullerene derivative acceptors for high performance polymer solar cells. *Phys. Chem. Chem. Phys.* **2011**, *13*, 1970−1983.
(10) Lin, Y.; Li, Y.; Zhan, X. Small molecule semiconductors for high-efficiency organic photovoltaics. *Chem. Soc. Rev.* **2012**, *41*, 4245−4272.
(11) Chen, J.; Cao, Y. Development of novel conjugated donor polymers for high-efficiency bulk-heterojunction photovoltaic devices. *Acc. Chem. Res.* **2009**, *42*, 1709−1718.
(12) Yan, C.; Barlow, S.; Wang, Z.; Yan, H.; Jen, A. K.-Y.; Marder, S. R.; Zhan, X. Non-fullerene acceptors for organic solar cells. *Nat. Rev. Mater.* **2018**, *3*, No. 18003.
(13) Geng, Y.; Tang, A.; Tajima, K.; Zeng, Q.; Zhou, E. Conjugated materials containing dithieno [3, 2-b: 2′, 3′-d] pyrrole and its derivatives for organic and hybrid solar cell applications. *J. Mater. Chem.* **2019**, *7*, 64−96.
(14) Frisch, M.; Trucks, G.; Schlegel, H.; Scuseria, G.; Robb, M.; Cheeseman, J.; Scalmani, G.; Barone, V.; Mennucci, B.; Petersson, G. Gaussian 09; Gaussian, Inc.2009, *32*, 5648−5652.
(15) Yang, Z.; Shao, C.; Cao, D. Screening donor groups of organic dyes for dye-sensitized solar cells. *RSC Adv.* **2015**, *5*, 22892−22898.
(16) Yang, Z.; Wang, D.; Bai, X.; Shao, C.; Cao, D. Designing triphenylamine derivative dyes for highly effective dye-sensitized solar cells with near-infrared light harvesting up to 1100 nm. *RSC Adv.* **2014**, *4*, 48750−48757.
(17) Ans, M.; Ayub, K.; Bhatti, I. A.; Iqbal, J. Designing indacenodithiophene based non-fullerene acceptors with a donor−acceptor combined bridge for organic solar cells. *RSC Adv.* **2019**, *9*, 3605−3617.
(18) Ans, M.; Manzoor, F.; Ayub, K.; Nawaz, F.; Iqbal, J. Designing dithienothiophene (DTT)-based donor materials with efficient photovoltaic parameters for organic solar cells. *J. Mol. Model.* **2019**, *25*, No. 222.
(19) Ans, M.; Iqbal, J.; Eliasson, B.; saif, M. J.; Ayub, K. Opto-electronic properties of non-fullerene fused-undecacyclic electron acceptors for organic solar cells. *Comput. Mater. Sci.* **2019**, *159*, 150−159.
(20) Ans, M.; Ayub, K.; Muhammad, S.; Iqbal, J. Development of fullerene free acceptors molecules for organic solar cells: a step way forward toward efficient organic solar cells. *Comput. Theor. Chem.* **2019**, *1161*, 26−38.
(21) Yang, Z.; Liu, C.; Shao, C.; Zeng, X.; Cao, D. Screening π-conjugated bridges of organic dyes for dye-sensitized solar cells with panchromatic visible light harvesting. *Nanotechnology* **2016**, *27*, No. 265701.
(22) Yang, Z.; Liu, Y.; Liu, C.; Lin, C.; Shao, C. TDDFT screening auxiliary withdrawing group and design the novel DA-π-A organic dyes based on indoline dye for highly efficient dye-sensitized solar cells. *Spectrochim. Acta, Part A* **2016**, *167*, 127−133.
(23) Barone, V.; Cossi, M. Quantum calculation of molecular energies and energy gradients in solution by a conductor solvent model. *J. Phys. Chem. A* **1998**, *102*, 1995−2001.
(24) Tang, S.; Zhang, J. Design of donors with broad absorption regions and suitable frontier molecular orbitals to match typical acceptors via substitution on oligo (thienylenevinylene) toward solar cells. *J. Comput. Chem.* **2012**, *33*, 1353−1363.
(25) Sattar, A.; Hussain, R.; Ishaq, S.; Assiri, M. A.; Imran, M.; Hussain, A.; Yawer, M. A.; Jan, S.; Hussain, R.; Mehboob, M. Y.; Khalid, M.; Ayub, K. Nonfullerene Near-Infrared Sensitive Acceptors "Octacyclic Naphtho [1, 2-b: 5, 6-b] Dithiophene Core" for Organic Solar Cell Applications: In Silico Molecular Engineering. *ACS Omega* **2022**, 16716−16727.
(26) Goszczycki, P.; Stadnicka, K.; Brela, M. Z.; Grolik, J.; Ostrowska, K. Synthesis, crystal structures, and optical properties of the π-π interacting pyrrolo [2, 3-b] quinoxaline derivatives containing 2-thienyl substituent. *J. Mol. Struct.* **2017**, *1146*, 337−346.
(27) Khan, M. U.; Iqbal, J.; Khalid, M.; Hussain, R.; Braga, A. A. C.; Hussain, M.; Muhammad, S. Designing triazatruxene-based donor materials with promising photovoltaic parameters for organic solar cells. *RSC Adv.* **2019**, *9*, 26402−26418.
(28) Li, Y.; Mi, L.; Wang, H.; Li, Y.; Liang, J. Design, electron transfer process, and opto-electronic property of solar cell using triphenylamine-based D-π-A architectures. *Materials* **2019**, *12*, No. 193.
(29) Mishra, R.; Regar, R.; Singh, V.; Panini, P.; Singhal, R.; Keshtov, M. L.; Sharma, G. D.; Sankar, J. Modulation of the power conversion efficiency of organic solar cells via architectural variation of a promising non-fullerene acceptor. *J. Mater. Chem.* **2018**, *6*, 574−582.
(30) Köse, M. E.; Mitchell, W. J.; Kopidakis, N.; Chang, C. H.; Shaheen, S. E.; Kim, K.; Rumbles, G. Theoretical studies on conjugated phenyl-cored thiophene dendrimers for photovoltaic applications. *J. Am. Chem. Soc.* **2007**, *129*, 14257−14270.
(31) Adnan, M.; Iqbal, J.; BiBi, S.; Hussain, R.; Akhtar, M. N.; Rashid, M. A.; Eliasson, B.; Ayub, K. Fine tuning the optoelectronic properties of triphenylamine based donor molecules for organic solar cells. *Z. Phys. Chem.* **2017**, *231*, 1127−1139.
(32) Irfan, M.; Iqbal, J.; Sadaf, S.; Eliasson, B.; Rana, U. A.; Ud-din Khan, S.; Ayub, K. Design of donor−acceptor−donor (D−A−D) type small molecule donor materials with efficient photovoltaic parameters. *Int. J. Quantum Chem.* **2017**, *117*, No. e25363.
(33) Li, Y. Molecular design of photovoltaic materials for polymer solar cells: toward suitable electronic energy levels and broad absorption. *Acc. Chem. Res.* **2012**, *45*, 723−733.
(34) Scharber, M. C.; Mühlbacher, D.; Koppe, M.; Denk, P.; Waldauf, C.; Heeger, A. J.; Brabec, C. J. Design rules for donors in bulk-heterojunction solar cells—Towards 10% energy-conversion efficiency. *Adv. Mater. Lett.* **2006**, *18*, 789−794.
(35) Naeem, M.; Jabeen, S.; Khera, R. A.; Mubashar, U.; Iqbal, J. Tuning of optoelectronic properties of triphenylamines-based donor materials for organic solar cells. *J. Theor. Comput. Chem.* **2019**, *18*, No. 1950036.
(36) Dkhissi, A. Excitons in organic semiconductors. *Synth. Met.* **2011**, *161*, 1441−1443.
(37) Kim, B. G.; Zhen, C. G.; Jeong, E. J.; Kieffer, J.; Kim, J. Organic Dye Design Tools for Efficient Photocurrent Generation in Dye-Sensitized Solar Cells: Exciton Binding Energy and Electron Acceptors. *Adv. Funct. Mater.* **2012**, *22*, 1606−1612.
(38) Sivakumar, G.; Paramasivam, M.; Bharath, D.; Rao, V. J. Energy level tuning of 'Z'-shaped small molecular non-fullerene electron acceptors based on a dipyrrolo [2, 3-b: 2′, 3′-e] pyrazine-2, 6 (1 H, 5 H)-dione acceptor unit for organic photovoltaic applications: A joint

https://doi.org/10.1021/acsomega.2c06878
ACS Omega 2023, 8, 1430−1442

experimental and DFT investigation on the effect of fluorination. *New J. Chem.* **2019**, *43*, 5173−5186.

https://doi.org/10.1021/acsomega.2c06878
ACS Omega 2023, 8, 1430−1442